by the superconducting fluctuation, and the attractive interaction for the d-wave Cooper pairing can be preserved. Thus, the two kinds of the fluctuations can coexist. And they will collaborate to develop the correlation of the d-wave superconductivity. These expectations are to be verified in the future.

Acknowledgement

The authors are grateful to Prof. K. Asayama, Prof. K. Machida, Prof. M. Ido, Prof. M. Oda, Prof. D. Hirashima, Prof. Y. Ohashi, Dr. K. Ishida, Dr. M. Ichioka, Dr. H. Kontani, Dr. T. Takimoto, Dr. A. Kobayashi, Dr. T. Ichinomiya, Mr. Y. Yanase and Mr. T. Jujo for their useful comments and fruitful discussions. The computation in this work has been done using the facilities of the Supercomputer Center, Kyushu University, Kyoto University, and Institute for Solid State Physics, University of Tokyo. The present work has been supported by a Grant-in-Aid for Scientific Research from the Ministry of Education, Science, Sports and Culture, Japan. One of the authors (S. K.) has been suported by a Research Fellowships of the Japan Society for the Promotion of Science for Young Scientists.

1) Y. Itoh, T. Machi, A. Fukuoka, K. Tanabe and H. Yasuoka: J. Phys. Soc. Jpn. **65** (1996) 3751.
2) K. Ishida, K. Yoshida, T. Mito, Y. Tokunaga, Y. Kitaoka, K. Asayama, Y. Nakayama, J. Shimoyama and K. Kishio: Phys. Rev. B **58** (1998) R5960.
3) B. Batlogg, H. Y. Hwang, H. Takagi, R. J. Cava, H. L. Kao and J. Kwo: Physica C **235–240** (1994) 130.
4) J. W. Loram, K. A. Mirza, J. M. Wade, J. R. Cooper and W. Y. Liang: Physica C **235–240** (1994) 134.
5) J. W. Loram, K. A. Mirza, J. R. Cooper and J. L. Tallon: Physica C **282–287** (1997) 1405.
6) T. Startseva, T. Timusk, A. V. Puchkov, D. N. Basov, H. A. Mook, M. Okuya, T. Kimura and K. Kishio: Phys. Rev. B **59** (1999) 7184.
7) Ch. Renner, B. Revaz, J.-Y. Genoud, K. Kadowaki and Ø. Fisher: Phys. Rev. Lett. **80** (1998) 149; Ch. Renner, B. Revaz, K. Kadowaki, I. Maggio-Aprole and Ø. Fisher: *ibid.* **80** (1998) 3606.
8) H. Ding, T. Yokoya, J. C. Campuzano, T. Takahashi, M. Randeria, M. R. Norman, T. Mochiku, K. Kadowaki and J. Giapintzakis: Nature **382** (1996) 51.
9) A. G. Loeser, Z.-X. Shen, D. S. Dessau, D. S. Marshall, C. H. Park, P. Fournier and A. Kapitulnik: Science **273** (1996) 325.
10) M. R. Norman, H. Ding, M. Randeria, J. C. Campuzano, T. Yokoya, T. Takeuchi, T. Takahashi, T. Mochiku, K. Kadowaki, P. Guptasarma and D. G. Hinks: Nature **392** (1998) 157.
11) P. Nozières and S. Schmitt-Rink: J. Low Temp. Phys. **59** (1985) 195.
12) S. Schmitt-Rink, C. M. Varma and A. E. Ruckenstein: Phys. Rev. Lett. **63** (1989) 445.
13) A. Tokumitu, K. Miyake and K. Yamada: Prog. Theor. Phys. Suppl. **106** (1991) 63.
14) C. A. R. Sá de Melo, M. Randeria and J. R. Engelbrecht: Phys. Rev. Lett. **71** (1993) 3202.
15) S. Koikegami and K. Yamada: J. Phys. Soc. Jpn. **67** (1998) 1114.
16) A. Kobayashi, A. Tsuruta, T. Matsuura and Y. Kuroda: J. Phys. Soc. Jpn. **67** (1998) 2626.
17) R. Haussmann: Phys. Rev. B **49** (1994) 12975.
18) R. Micnas, M. H. Pedersen, S. Schafroth, T. Schneider, J. J. Rodríguez-Núñez and H. Beck: Phys. Rev. B **52** (1995) 16223.
19) J. R. Engelbrecht, A. Nazarenko, M. Randeria and E. Dagotto: Phys. Rev. B **57** (1998) 13406.
20) J. Mary, B. Jankó and K. Levin: Phys. Rev. B **59** (1999) 1534; Q. Chen, I. Kosztin, B. Jankó and K. Levin: *ibid.* **59** (1999) 7083.
21) T. Ichinomiya and K. Yamada: J. Phys. Soc. Jpn. **68** (1999) 981.
22) T. Jujo and K. Yamada: J. Phys. Soc. Jpn. **68** (1999) 2198.
23) A. Kobayashi, A. Tsuruta, T. Matsuura and Y. Kuroda: J. Phys. Soc. Jpn. **68** (1999) 2506.
24) Y. Yanase and K. Yamada: J. Phys. Soc. Jpn. **68** (1999) 2999.
25) T. Dahm, D. Manske and L. Tewordt: Phys. Rev. B **55** (1997) 15274.
26) N. E. Bickers, D. J. Scalapino and S. R. White: Phys. Rev. Lett. **62** (1989) 961; N. E. Bickers and D. J. Scalapino: Ann. Phys. (N.Y.) **193** (1989) 206.
27) P. Monthoux and D. J. Scalapino: Phys. Rev. Lett. **72** (1994) 1874.
28) C.-H. Pao and N. E. Bickers: Phys. Rev. B **49** (1994) 1586; Phys. Rev. Lett. **72** (1994) 1870; Phys. Rev. B **51** (1995) 16310.
29) T. Dahm and L. Tewordt: Phys. Rev. Lett. **74** (1995) 793; Phys. Rev. B **52** (1995) 1297; Physica C **246** (1995) 61; T. Dahm, D. Manske and L. Tewordt: Phys. Rev. B **54** (1996) 602.
30) J. W. Serene and D. W. Hess: Phys. Rev. B **44** (1991) 3391; J. J. Deisz, D. W. Hess and J. W. Serene: Phys. Rev. Lett. **76** (1996) 1312; D. W. Hess, J. J. Deisz and J. W. Serene: Phil. Mag. **74** (1996) 457.
31) R. Putz, R. Preuss, A. Muramatsu and W. Hanke: Phys. Rev. B **53** (1996) 5133.
32) A. I. Liechtenstein, O. Gunnarsson, O. K. Andersen and R. M. Martin: Phys. Rev. B **54** (1996) 12505.
33) S. Grabowski, M. Langer, J. Schmalian and K. H. Bennemann: Europhys. Lett. **34** (1996) 219; S. Grabowski, J. Schmalian, M. Langer and K. H. Bennemann: Phys. Rev. B **55** (1997) 2784; J. Schmalian, S. Grabowski and K. H. Bennemann: Phys. Rev. B **56** (1997) R509.
34) S. Koikegami, S. Fujimoto and K. Yamada: J. Phys. Soc. Jpn. **66** (1997) 1438.
35) T. Takimoto and T. Moriya: J. Phys. Soc. Jpn. **66** (1997) 2459; *ibid.* **67** (1998) 3570.
36) J. Schmalian: Phys. Rev. Lett. **81** (1998) 4232.
37) H. Kino and H. Kontani: J. Phys. Soc. Jpn. **67** (1998) 3691.
38) H. Kondo and T. Moriya: J. Phys. Soc. Jpn. **67** (1998) 3695.
39) H. Kontani and K. Ueda: Phys. Rev. Lett. **80** (1998) 5619.
40) O. K. Anderson, O. Jepsen, A. I. Liechtenstein and I. I. Mazin: Phys. Rev. B **49** (1994) 4145.
41) G.-q. Zheng, Y. Kitaoka, K. Asayama, K. Hamada, H. Yamauchi and S. Tanaka: Physica C **260** (1996) 197.
42) H. J. Vidberg and J. W. Serene: J. Low Temp. Phys. **29** (1977) 179.
43) M. Arai, T. Nishijima, Y. Endoh, T. Egami, S. Tajima, K. Tomimoto, Y. Shiohara, M. Takahashi, A. Garrett and S. M. Bennington: Phys. Rev. Lett. **83** (1999) 608.

Journal of the Physical Society of Japan
Vol. 69, No. 3, March, 2000, pp. 777-784

Electronic Structure and Electrical Conductivity of Amorphous Si–Ti Alloys Manifesting the Metal-Insulator Transition

Katsuya KAWADE, Atsuko SUZUKI and Kazuhide TANAKA*

Department of Materials Science and Engineering, Nagoya Institute of Technology, Showa-ku, Nagoya 466-8555

(Received October 7, 1999)

The electrical conductivity σ of amorphous $Si_{100-x}Ti_x$ alloys prepared by ion-beam sputtering has been measured over a temperature range between 4.2 and 290 K. The temperature dependence of σ is well expressed by a formula derived by the variable-range hopping theory with an exponent $n \sim 0.40$ for $x \leq 11.5$, whereas, for $x \geq 12.8$, it is better expressed by a formula describing the conduction by electrons liberated from weakly localized states through inelastic electron-electron scattering. Thus, the metal-insulator transition takes place at $11.5 < x_c < 12.8$ in this system. The electronic structure of these alloys has been studied by measuring XPS and UPS spectra. Furthermore, DV-Xα calculation has been carried out for certain Si–Ti alloy clusters of diamond structure to simulate the electronic structure of the amorphous alloys. The calculated total and partial density of states well reproduces the features of the photoemission spectra. The calculation also provides information on the localization of electronic states in the amorphous alloys.

KEYWORDS: amorphous Si–Ti alloys, electrical conductivity, metal-insulator transition, variable-range hopping, localization, XPS and UPS, DV-Xα cluster calculation

§1. Introduction

The structure, stability and electronic properties of semiconductor (Si, Ge)-transition-metal (TM) alloys have long been the subjects of a number of investigations. For understanding the characteristic properties of the alloys, many experimental and theoretical studies have been carried out, among which those revealing the nature of chemical bonding in TM silicides appear to be fundamentally most important.[1,2] A stable crystalline silicide is readily formed in a stoichiometric composition at a contact interface between Si and a TM when the couple is annealed at an appropriate temperature, and it is known to provide a good ohmic contact between them.[3] In addition, the formation of a non-stoichiometric solid solution of Si and a TM is also important in the semiconductor technology. It is readily formed by coevaporation or cosputtering onto a substrate, although it usually takes a metastable amorphous structure. The atomic structure,[4] thermal stability[5] and electronic properties[6,7] of amorphous Si-TM alloys have also been studied and their bonding characteristics have been revealed. Specifically, much attention has been payed to Ti-silicides in crystalline and amorphous forms in recent years[8-11]

The objective of the present study is to make clear the electronic structure and electronic transport properties of amorphous Si–Ti alloys over a wide range of composition. Amorphous Si(or Ge)-TM alloys manifest the metal-insulator transition (MIT) at a critical concentration x_c of the TM which usually falls between ~10 and ~15 at.%. This transition, called Anderson transition, has long been investigated for a variety of alloy systems and its mechanisms have been theoretically explored.[12-15] We have investigated the MIT effects in amorphous Si-Pd,[16] Si-Ni,[17] Ge-Ag[18] and Ge-Pd[19,20] alloys, and related them with the bandstructure or bonding characteristics of the alloys as revealed by photoemission spectroscopy. The reason for choosing the Si–Ti system in this study is as follows. Firstly, the MIT of this system has not been studied in detail in the past; secondly, this system has an advantage of providing homogeneous amorphous alloys over a much wider composition range than any other systems studied to date; and thirdly, since both Si and Ti are tetravalent, unique bonding characteristics and hence unique MIT effect may be expected for this system in comparison with the others.

In this study, we first make clear the MIT effect in Si–Ti amorphous alloys by electrical conductivity measurements and determine the critical concentration x_c. We next reveal their electronic structures by XPS and UPS measurements. Finally, we calculate the electronic structure of Si–Ti alloy clusters by DV-Xα molecular orbital method and discuss the relationship between the MIT and electronic structure in this system.

§2. Experimental Procedure

The samples used in this experiment were prepared by Ar-ion-beam sputtering in a similar way as described previously.[16-19] Briefly, a composite target of high-purity Si and 99.9% Ti chips of appropriate area ratio was simultaneously sputtered and deposited on a Si(111) or a quartz glass substrate to a film thickness of about 1 μm at ambient temperature. The former was used for photoemission study and the latter for electrical conductivity measurements. The alloy phases formed were

* E-mail: tanaka@mse.nitech.ac.jp

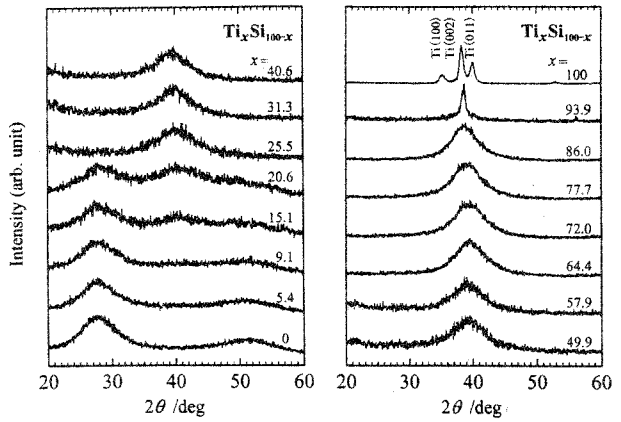

Fig. 1. X-ray diffraction patterns (CuKα) of sputter-deposited $Si_{100-x}Ti_x$ alloys measured in the grazing-incidence mode.

checked with both conventional ($\theta/2\theta$ scan) and grazing-incidence (2θ scan) X-ray diffraction using CuKα radiation. The chemical composition of each sample was determined with EDX analysis at 5 kV. Photoemission spectra were measured with XPS and UPS apparatus with monochromated AlKα and HeI photon sources, respectively. The DC conductivity was measured with a two-probe method over a temperature range between 4.2 and 290 K. The method of measuring the photoemission spectra has been described elsewhere.[17,20]

Figure 1 shows XRD patterns of $Si_{100-x}Ti_x$ alloys measured in the grazing-incidence mode, from which we can recognize that amorphous alloys are formed over the composition $0 \leq x \leq 86.0$. The evolution of halo peaks of the amorphous structure with Ti concentration is very similar to those observed in other alloy systems. It suggests that the tetrahedral random network of amorphous Si is gradually modified into a metallic random close-packing structure with addition of Ti. These amorphous alloys are structurally stable and crystallize at 600–900 K depending on the Ti concentration.[11]

§3. Results and Discussion

3.1 *Electrical conductivity*

Figure 2 shows the DC conductivity σ plotted against temperature T in a log-log scale for amorphous $Si_{100-x}Ti_x$ alloys with $x = 0$–20.0. It can be seen from this figure that σ changes characteristically with temperature and Ti concentration. For lower concentrations, $x \lesssim 11.5$, it varies strongly depending on T like a semiconductor or an insulator, whereas for higher concentrations, $x \gtrsim 12.8$, its temperature dependence becomes much less strong, behaving like an amorphous metallic alloy.

3.1.1 *Insulating region*

According to Mott's variable-range hopping (VRH) theory[12-14] of electrical conduction on the insulating side of the metal-insulator transition, the conductivity is given by

$$\sigma = \sigma_0 \exp\left[-\left(\frac{T_0}{T}\right)^n\right], \tag{1}$$

where σ_0 and T_0 are numerical parameters that involve

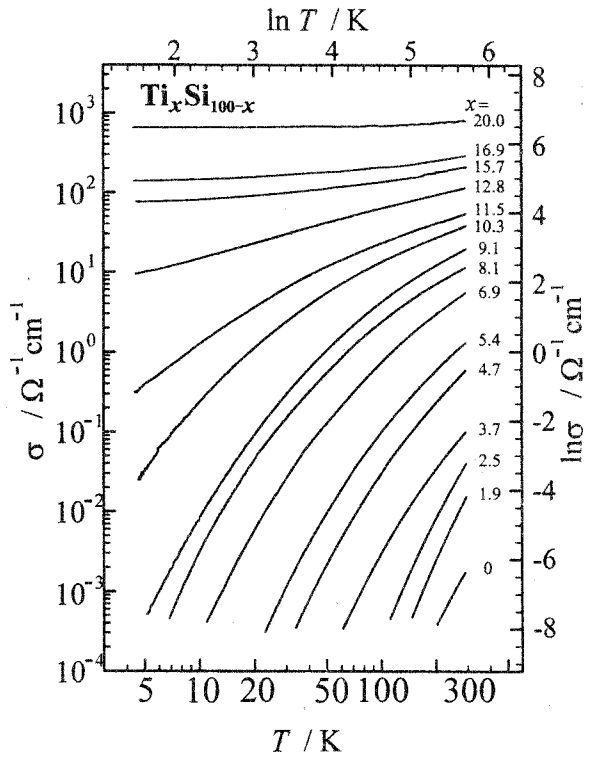

Fig. 2. DC conductivity σ plotted against temperature T in a log-log scale for amorphous $Si_{100-x}Ti_x$ alloys with $x = 0$–20.0.

the sample variables, and n is an index that reflects the dimensionality of the sample. The parameters σ_0 and T_0 are expressed as follows:

$$\sigma_0 \approx 0.03e^2/\hbar L_i, \tag{2}$$

and

$$T_0 = 24\alpha^3/\pi k_B N(E_F), \tag{3}$$

where L_i is an inelastic diffusion length of an electron, α is the inverse length of a localized wave function denoting the degree of localization, $N(E_F)$ is the density of states (DOS) at the Fermi level E_F, and the remaining quantities have their usual meanings. As for the exponent, $n = 1/4$ is predicted for the three-dimensional (3D) hopping of electrons over the localized states with a flat DOS at E_F, whereas $n = 1/3$ results for the 2D hopping. These equations have been derived neglecting the electron-electron Coulomb interaction among the hopping electrons.

However, Efros and Shklovskii[21] have shown that, by including the electron-hole interaction on the localized states, a Coulomb gap Δ opens just at E_F and the DOS is no longer flat but tends to zero at E_F. In their modified VRH theory, σ is still given by eq. (1), but T_0 is replaced by

$$T_0 = \alpha e^2/\kappa, \tag{4}$$

with κ the dielectric constant and, furthermore, $n = 1/2$ is predicted irrespectively of the dimensionality of the sample.

Now, we examine whether the DC conductivity of

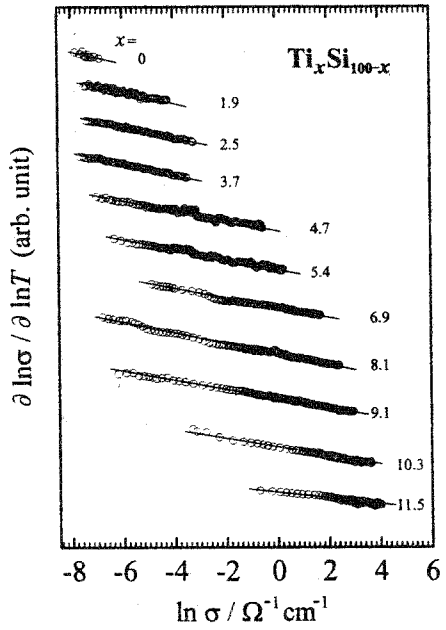

Fig. 3. Relationship between $\partial \ln\sigma/\partial \ln T$ and $\ln\sigma$ for $0 \leq x \leq 11.5$.

Table I. Values of n, σ_0 and T_0 involved in eq. (1) obtained by the least-squares fitting to the experimental data for amorphous $Si_{100-x}Ti_x$ alloys.

Composition, x	n	$\sigma_0/\Omega^{-1}\mathrm{cm}^{-1}$	T_0/K
0	0.320	3.90×10^3	1.15×10^6
1.9	0.383	1.35×10^3	1.69×10^5
2.5	0.389	7.21×10^2	1.05×10^5
3.7	0.395	0.77×10^2	3.52×10^4
4.7	0.387	1.37×10^2	2.44×10^4
5.4	0.385	1.70×10^2	1.84×10^4
6.9	0.393	2.00×10^2	9.84×10^3
8.1	0.390	2.41×10^2	5.10×10^3
9.1	0.359	5.51×10^2	8.34×10^3
10.3	0.341	4.02×10^2	3.66×10^3
11.5	0.252	8.40×10^2	1.61×10^4

amorphous $Si_{100-x}Ti_x$ obeys the VRH theory in the semiconducting region. To facilitate the comparison, eq. (1) is arranged to give

$$\frac{\partial \ln\sigma}{\partial \ln T} = n(\ln\sigma_0 - \ln\sigma), \tag{5}$$

and we check whether the linearity between $\partial \ln\sigma/\partial \ln T$ and $\ln\sigma$ is actually satisfied or not. Figure 3 shows the relationship between the two quantities for $0 \leq x \leq 11.5$, from which we can confirm that eq. (5) is really satisfied. The values of n, σ_0 and T_0 obtained by least-squares fitting are given in Table I. We find that, in most of these alloys (excluding $x = 11.5$), $n \sim 0.40$ and $\sigma_0 = 10^2$–$10^3\,\Omega^{-1}\mathrm{cm}^{-1}$ are realized. On the other hand, T_0 changes systematically with the Ti concentration; it decreases from $\sim 10^6$ to $\sim 10^3$ K with increasing x. The n-value falls intermediate between those of Mott's and Efros and Shklovskii's theories. The systematic decrease of T_0 with x can be explained by the delocalization of electronic states (decrease in α) and increase in $N(E_F)$ on the basis of Mott's theory, or by the decrease in α and increase in κ on the basis of Efros and Shklovskii's theory. The changes in $N(E_F)$ and the degree of localization of electronic states with Ti concentration will be discussed in the following sections.

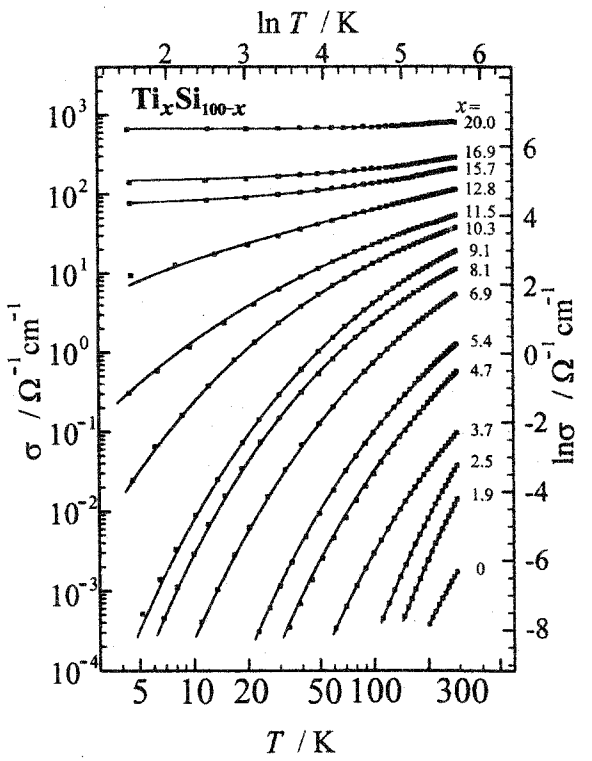

Fig. 4. Comparison between the fitted theoretical curves of eq. (2) (solid lines) with the measured ones (dots) for the alloys with $0 \leq x \leq 11.5$.

Figure 4 shows a comparison of the fitted theoretical curves of eq. (2) (solid lines) with the measured ones (dots) for the alloys with $0 \leq x \leq 11.5$. The agreement between the theory and experiment is quite satisfactory throughout the measured temperature range.

3.1.2 *Metallic region*

The electrical conductivity of a disordered allloy on the metallic side is described in terms of two main contributions.[15,22] One is the conduction induced by an anomaly in DOS at E_F due to electron-electron Coulomb interaction, called Altshuler and Aronov effect,[23] and the other is that associated with weak localization, which describes the conduction of electrons liberated from weakly localized states via inelastic electron-electron scattering. The conductivity is simply expressed as

$$\sigma = \sigma(0) + aT^{1/2} + bT, \tag{6}$$

where, $\sigma(0)$ is a residual conductivity at $T = 0$, and the second and third terms correspond to the Altshuler and Aronov effect and weak localization effect, respectively, with a and b numerical parameters independent of the temperature but dependent on the sample variables. This equation has been used to analyze the conductivity of amorphous $Si_{100-x}Ti_x$ for $x = 12.8$–20.0 shown in Fig. 2. The values of $\sigma(0)$, a and b for these alloys obtained by least-squares fitting are given in Table II. They vary systematically with the Ti concen-

Table II. Values of $\sigma(0)$, a and b involved in eq. (6) obtained by the least-squares fitting to the experimental data for amorphous $Si_{100-x}Ti_x$ alloys.

Composition, x	$\sigma(0)$/ $\Omega^{-1}cm^{-1}$	a/ $\Omega^{-1}cm^{-1}K^{-1/2}$	b/ $\Omega^{-1}cm^{-1}K^{-1}$
12.8	−7.76	7.00	0.010
15.7	66.6	4.77	0.217
16.9	139	3.73	0.301
20.0	673	−5.36	0.791

tration. In this analysis $\sigma(0)$ for $x = 12.8$ happens to take a negative value. This is physically unreasonable. To determine it accurately, σ should be measured down to far lower temperatures. The fitted curves are compared with the measured ones in Fig. 4. The agreement between the theory and experiment is again quite satisfactory except for $x = 12.8$ in the lowest temperature region. We close this section by concluding that the metal-insulator transition in amorphous $Si_{100-x}Ti_x$ alloys occurs at $11.5 < x_c < 12.8$.

3.2 Photoemission spectroscopy

Figure 5 shows XPS valence band spectra of amorphous $Si_{100-x}Ti_x$ alloys, excluding $x = 93.9$ and 100 which are crystalline, normalized to the respective maximum intensity. In pure amorphous Si ($x = 0$), broad valence band peaks consisting of Si3s and 3p states, together with a mixed 3s + 3p state inbetween, are seen in the range of binding energy $E_B = 0$–10 eV. With addition of Ti, the intensity near E_F ($E_B = 0$) which is minimal in pure Si increases developing into a discrete peak with a clear Fermi edge. This peak represents mainly Ti3d state in the alloy. In addition, peaks a and b develop in the Si(3s + 3p) region, as shown in the figure. In these spectra, the Si3s peak is more or less modified owing to the overlapping of Ar3p state which has been introduced into the sample during surface cleaning with Ar-ion sputtering. The effect of contamination of oxygen and carbon on these spectra is reduced to minimal by the cleaning except for the Ti-rich alloys.

Figure 6 shows UPS spectra of the alloys with $x =$ 0–25.5. These spectra are generally similar to those of XPS shown above. However, owing to the high sensitivity and resolution of UPS over XPS, the former provides spectral features near the Fermi level more clearly than the latter. Namely, the spectral intensity at E_F, which is minimal in pure amorphous Si, rises with a small addition of Ti and an abrupt Fermi edge becomes manifest for higher concentrations, indicating that the electronic structure changes from a semiconductor-like state to a metallic one by the alloying.

This process can be seen more clearly by observing the evolution of the Fermi edge with Ti concentration in more detail, as shown in Fig. 7, where the measured intensity is plotted against energy in a magnified scale for alloys of low Ti concentrations. Taking into account an energy resolution of 0.14 eV of the UPS, we can recognize from this figure that the Fermi edge just arises at $3.7 < x_m < 4.7$ and a metallic bandstructure is formed above this concentration. Since the MIT takes place at $11.5 < x_c < 12.8$ as shown in the previous section, electrons occupying the states in the vicinity of E_F are still localized and the metallic conduction is prohibited in alloys with $x_m < x < x_c$. This picture is similar to those in amorphous Si–Ni[17] and Ge–Pd[19,20] alloys. It is worth noting here that the present energy resolution of UPS is not enough to detect a Coulomb gap Δ formed at E_F as predicted by Efros and Shklovskii[21] for $x < x_c$. The magnitude of Δ would be as small as ∼10 meV or less, which is far smaller than ∼140 meV of the present spectral resolution.

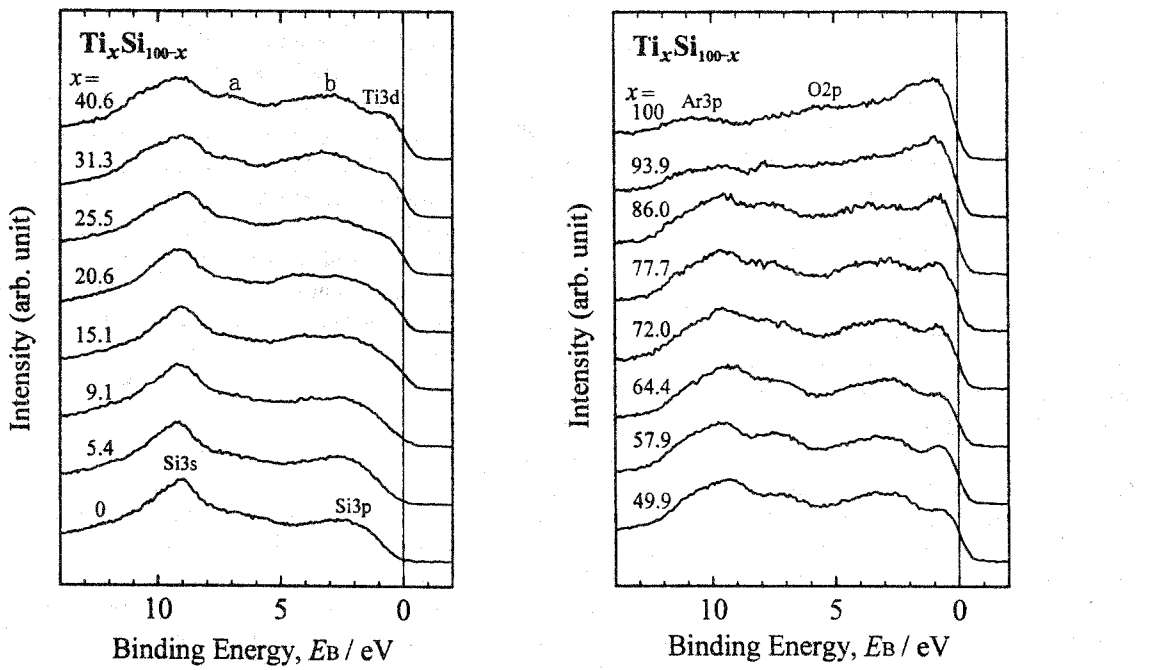

Fig. 5. XPS valence band spectra of amorphous $Si_{100-x}Ti_x$ alloys, excluding $x = 93.9$ and 100 which are crystalline, normalized to the respective maximum intensity.

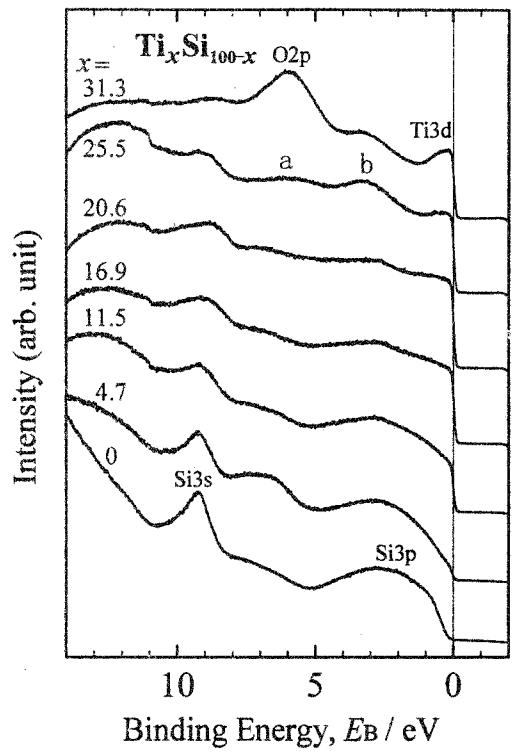

Fig. 6. UPS spectra of amorphous $Si_{100-x}Ti_x$ alloys with $x =$ 0–25.5.

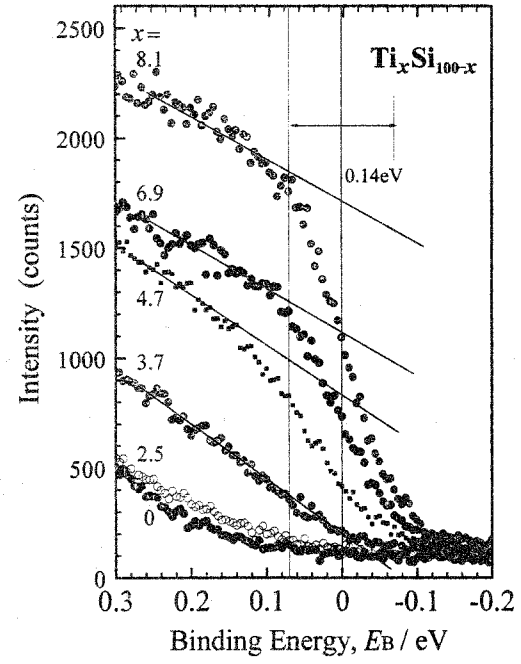

Fig. 7. Fermi-edge profiles of the UPS spectra for low Ti concentrations.

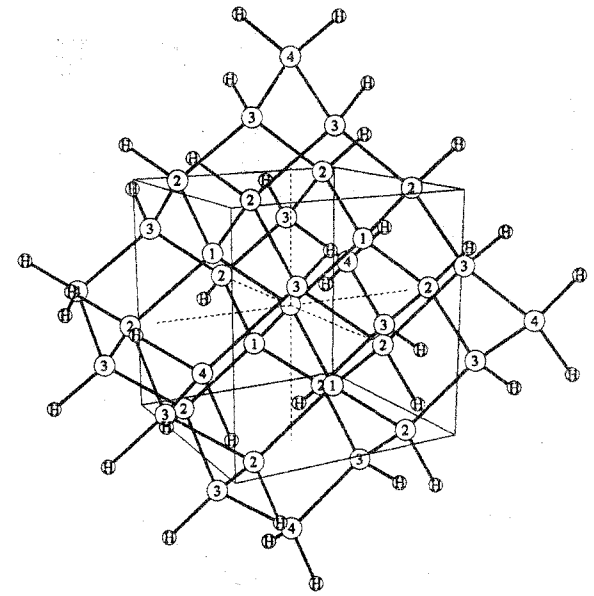

Fig. 8. The model cluster of Si_{35} of diamond structure used for the DV-Xα calculation. The number on each atom denotes the order of distance from the central atom.

3.3 DV-Xα cluster calculations

The photoemission spectra and the metal-insulator transition in amorphous Si–Ti alloys presented above may be understood more clearly by calculating their electronic structures. We attempt here, as a first step, to calculate the electronic structure of alloy clusters of diamond structure, instead of dealing with the real alloy structure seriously. This is partly supported by the fact that the structures of amorphous Si and Si–Ni alloys of low Ni concentrations (below ∼20 at.% Ni) resemble each other,[4] and are composed of tetrahedral random packing of covalently bonded Si atoms;[24] furthermore, the local structure of amorphous Si is similar to crystalline Si in the interatomic distance and coordination number.[25] The calculation has been performed by the DV-Xα molecular orbital method in a similar way as described elsewhere.[18,20]

Figure 8 shows the model cluster of Si_{35} used for the calculation, where thirty-five Si atoms are arranged in diamond structure together with thirty-six H atoms added to terminate the surface dangling bonds. This cluster is larger in size than the Ge_{17} cluster employed in the previous calculations.[18,20] The alloy clusters, $Si_{34}Ti$, $Si_{33}Ti_2$, $Si_{31}Ti_4$ and $Si_{30}Ti_5$, are obtained by substituting the respective number of Ti atoms for the central, two 1st-neighbor, four 1st-neighbor, and the central plus four 1st-neighbor Si atoms, respectively. The interatomic distances, $d_{Si-Si} = 0.235$ nm and $d_{Si-H} = 0.146$ nm, are taken to be consistent with those of Si crystal and SiH_4 molecule, respectively. In the DV-Xα calculation, the atomic orbitals (AOs) of H1s, Si3s to 3d and Ti3d to 4p, together with the respective inner core orbitals, are involved to constitute the molecular orbitals (MOs) of these clusters.

Figure 9 shows the energy level diagram of MOs for these clusters, where the solid and dashed lines denote

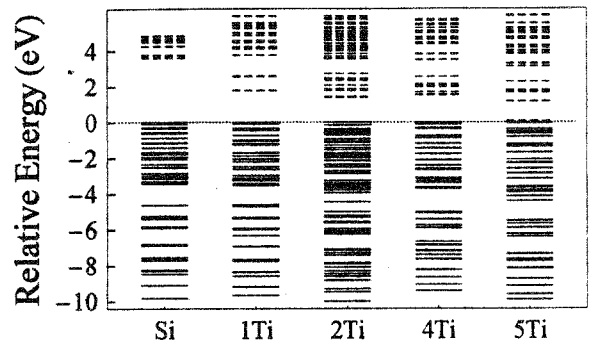

Fig. 9. The energy level diagram of the molecular orbitals for the Si_{35} clusters with 0 to 5 substituted Ti atoms.

occupied and unoccupied states, respectively, and the energy is measured relative to the highest occupied molecular orbital (HOMO) for each cluster. The lowest unoccupied molecular orbital (LUMO), which is located at 3.6 eV for Si_{35}, is continually lowered with increasing number of Ti atoms and nearly comes into contact with the HOMO for $Si_{30}Ti_5$.

Figures 10(a) to 10(c) shows the total and partial densities of states for the Si_{35}, $Si_{34}Ti$ and $Si_{31}Ti_4$ clusters, respectively, where the individual MO level is broadened with a Gaussian of 0.2 eV in full width at half maximum (FWHM). In this figure, the partial DOS of H1s is not displayed for the sake of clarity, and, furthermore, this component is not included in the total DOS to facilitate comparison with the photoemission spectra of amorphous Si–Ti alloys, as shown later. It can be seen from this figure that, in (a) Si_{35} cluster, the total DOS consists of upper Si3p and lower Si3s bands together with intermediate Si(3s + 3p) band in the occupied region, whereas Si(3p+3d) band is mainly involved in the unoccupied region, causing a band gap of ~2.7 eV in between. This band gap is wider than that for Si crystal (~1.2 eV), partly reflecting the small cluster size used in the present calculation. In (b) $Si_{34}Ti$ cluster, Ti3d state comes out at the top of the occupied band as well as within the band gap, both of which are coupled with Si3p and Si3d bands. In (c) $Si_{31}Ti_4$ cluster, the Ti3d state at the top of the occupied band broadens to form a Ti3d band and mixes with the Si3p band, while the Ti3d state inside the band gap also grows and broadens to form a band and mixes with the Si3p and Si3d bands. In this cluster, the band gap appears to be almost closed. In Fig. 10(d), the total DOS of Si_{35} to $Si_{30}Ti_5$ clusters are displayed, from which we can recognize a continual variation of the electronic structure from a separated band of a semiconductor into a continuous metallic band with increasing number of Ti atom.

Figure 11 shows a comparison between the calculated total DOS for several Si–Ti alloy clusters and UPS spectra of amorphous Si–Ti alloys of comparable Ti concentrations. The Fermi level of each cluster (vertical dotted line) is chosen at the midpoint of the HOMO and LUMO energy levels. The DOS of the cluster is displayed after being broadened with a Gaussian of 0.5 eV in FWHM to facilitate the comparison. Since each photoemission spectrum implicitly involves photoionization cross-sections for the atomic states of Si and Ti that multiply the respective partial DOS, it does not always give the total DOS of the Si–Ti alloy. However, apart from the absolute spectral intensity, the calculated total DOS appears to reproduce the features of the measured UPS spectra satisfactorily, including the appearance of peaks *a* and *b*, for low Ti concentrations.

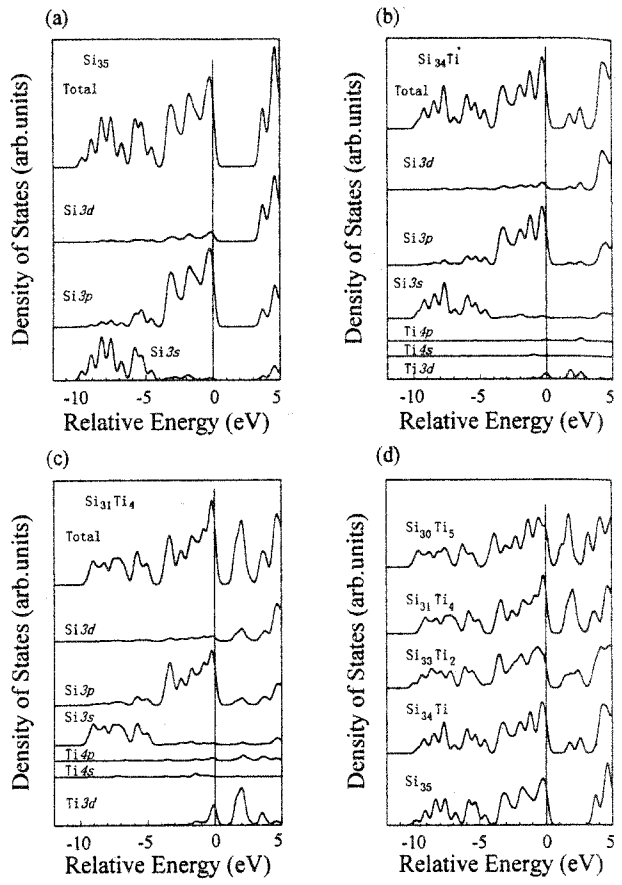

Fig. 10. The total and partial densities of states for (a) Si_{35}, (b) $Si_{34}Ti$ and (c) $Si_{31}Ti_4$ clusters, and (d) the set of total DOS for all the clusters studied.

From the calculated MOs for the alloy clusters, we can derive information on the localization of electronic states, which is an important aspect of the electronic states in a disordered alloy manifesting the metal-insulator transition. Figure 12 shows the energy distribution of the localization index (LI)[20] for the MOs of the clusters. The LI gives a degree of spread of a MO with respect to the AOs constituting the MO. It becomes largest when the MO is confined around certain atoms (fully localized), whereas it becomes smallest when the MO is extended equally over all the atoms pertaining to the MO (fully delocalized). It can be seen from the figure that the LI depends on the symmetry of MOs and becomes relatively large for energies in the vicinity of the band gap. A recent study on the localization of electronic states in pure amorphous Si also shows a similar trend of the LI distribution; that is, states close to band edges are more localized than ones far from the edges.[26] Another feature of the calculated LI is that it depends on the

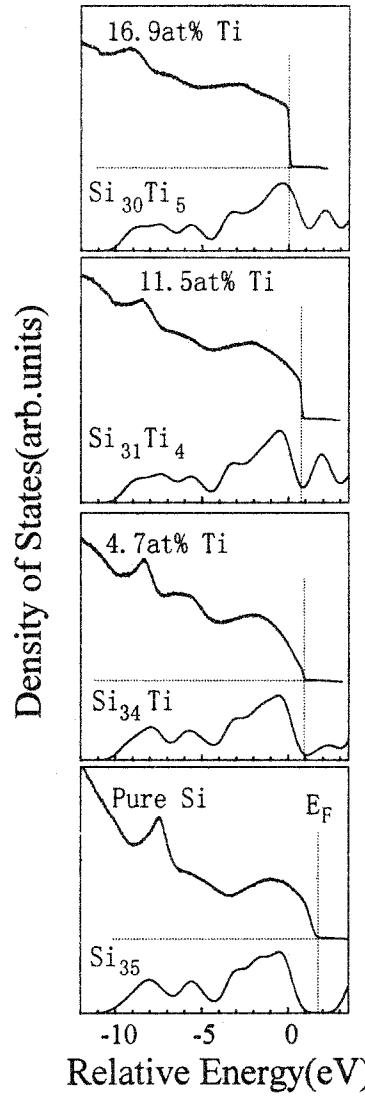

Fig. 11. Comparison between the calculated total DOS for alloy clusters and UPS spectra of amorphous alloys of comparable Ti concentrations.

number of Ti atoms in the clusters, as shown for HOMO and LUMO in Fig. 13. The LIs become largest upon substituting one Ti atom for Si but decrease with further increase in Ti atoms. It is evident that Ti3d states are involved to cause the above behavior of the LIs; the MOs around the band gap tend to be delocalized when the Ti–Ti interaction is increased.

Incidentally, the above result on the localization of MOs in the clusters is not directly applicable to the MIT effect in amorphous Si–Ti alloys. In a real disordered alloy, the localization of electronic states takes place when a relation $k_F l \sim 1$ is satisfied between the Fermi wave number k_F and the mean free-path l of a conduction electron in the alloy (Ioffe-Regel condition).[27] This relation, which is essential to the electron transport in amorphous alloys undergoing the MIT, is out of consideration in this study. Therefore, it is not possible to argue quantitatively a relationship between the electron localization and the MIT in amorphous Si–Ti alloys based on the present cluster calculation. However,

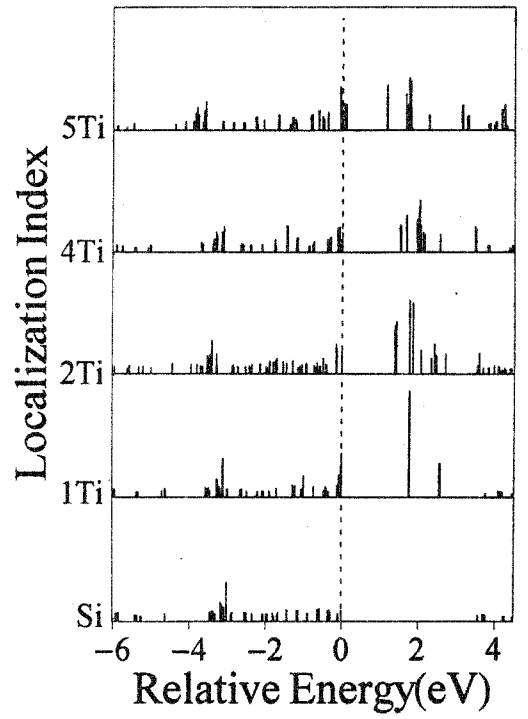

Fig. 12. The distribution of localization indices for the MOs of the clusters.

Fig. 13. The variation of the localization indices for the HOMO and LUMO with the number of Ti atoms in the clusters.

it may provide a qualitative account on the variation of the degree of electron localization with Ti concentration, which has really been observed by the conductivity measurements through the change in T_0, and hence α, via eqs. (3) and (4).

§4. Summary and Conclusions

(1) Homogeneous $Si_{100-x}Ti_x$ amorphous alloys can be readily produced by ion-beam sputtering over a wide range of composition ($0 \leq x \leq 86.0$) at ambient temperatures. The DC conductivity of the alloy at temperatures between 4.2 and 290 K well obeys eq. (1), derived

on the basis of the variable-range hopping theory, on the insulating side of the metal-insulator transition ($x < x_c$) where $11.5 < x_c < 12.8$. The exponent $n \sim 0.40$ in this equation is intermediate between one ($n = 1/4$) derived in Mott's original VRH theory and another ($n = 1/2$) predicted by Efros and Shklofskii taking into account the Coulomb interaction between localized electron-hole pairs. On the other hand, on the metallic side ($x > x_c$), it well obeys eq. (6) describing the conduction by electrons liberated from weakly localized states by inelastic electron-electron scattering.

(2) The electronic structure of pure amorphous Si as revealed by XPS and UPS consists of broad well-separated 3s and 3p bands, together with a mixed 3s+3p band inbetween. With addition of Ti, the Si3p band is strongly modified by mixing with Ti3d band which develops just below E_F. A close examination of the evolution of the UPS Fermi edge with Ti concentration indicates that the band gap of amorphous Si is removed for $x > x_m$ ($3.7 < x_m < 4.7$), and a metallic bandstructure is formed.

(3) To understand the electronic structure and MIT in amorphous Si–Ti alloys, DV-Xα calculations are performed for model clusters, such as Si_{35}, $Si_{34}Ti$, $Si_{33}Ti_2 \cdots Si_{30}Ti_5$ with diamond structure. The calculated total DOS for the clusters well explains the features of the bandstructure of amorphous alloys as revealed by XPS and UPS, including the removal of the band gap above a low Ti concentration. The calculation also provides information on the localization of electronic states in the amorphous alloy. The degree of localization of HOMO and LUMO tends to decrease with increasing number of Ti atoms in the clusters. This trend is consistent with the results of conductivity which show, with the help of VRH theory, that the degree of localization is reduced as the Ti concentration approaches the critical concentration x_c for the metal-insulator transition.

Acknowledgements

We acknowledge Professor M. Morinaga and Dr. H. Yukawa of Nagoya University for permitting us to use their computing facility and DV-Xα program. We also acknowledge the Instrumental Center, Institute for Molecular Science, for the use of a UPS apparatus (VG ESCALAB MKII). The cooperation of Mr. M. Yamada and Mr. H. Takaki in measuring the photoemission spectra is acknowledged.

1) J. H. Weaver, A. Franciosi and V. L. Moruzzi: Phys. Rev. B **29** (1984) 3293.
2) P. J. W. Weijs, H. Van Leuken, R. A. de Groot, J. C. Fuggle, S. Reiter, G. Wiech and K. H. J. Buschow: Phys. Rev. B **44** (1991) 8195.
3) A. Hiraki: Surf. Sci. Rep. **3** (1984) 357.
4) P. Ballone and S. Rubini: Phys. Rev. B **51** (1995) 14962.
5) J. R. A. Carlsson, J.-E. Sundgren, X.-H. Li, L. D. Madsen and H. T. G. Hentzell: J. Appl. Phys. **81** (1997) 1150.
6) K. Söldner, A. Grassmann, G. Saemann, W. Zahorowski, A. Simnnek and G. Wiech: Z. Phys. B **75** (1989) 59.
7) K. Tanaka, T. Saito, K. Suzuki and R. Hasegawa: Phys. Rev. B **32** (1985) 6853.
8) P. J. W. Weijs, M. T. Cryzyk, J. C. Fuggle, W. Speier, D. D. Sarma and K. H. J. Buschow: Z. Phys. B **78** (1990) 423.
9) M. Ekman and V. Ozolins: Phys. Rev. B **57** (1998) 4419.
10) N. Zotov and D. Parlapanski: J. Mater. Sci. **29** (1994) 2813.
11) M. Naka, T. Matsui, M. Maeda and H. Mori: Mater. Trans. JIM **36** (1995) 797.
12) N. F. Mott and E. A. Davis: *Electronic Processes in Non-Crystalline Materials* (Clarendon, Oxford, 1979).
13) N. F. Mott: *Conduction in Non-Crystalline Materials* (Clarendon, Oxford, 1987).
14) N. F. Mott: *Metal-Insulator Transitions* (Taylor & Francis, London, 1990).
15) P. A. Lee and T. V. Ramakrishnan: Rev. Mod. Phys. **57** (1985) 287.
16) K. Tanaka, K. Furui and M. Yamada: J. Phys. Soc. Jpn. **64** (1995) 4790.
17) A. Isobe, M. Yamada and K. Tanaka: J. Phys. Soc. Jpn. **66** (1997) 2103.
18) A. Suzuki and K. Tanaka: Jpn. J. Appl. Phys. **37** (1998) 4872.
19) A. Endo, A. Suzuki and K. Tanaka: J. Phys. Soc. Jpn. **68** (1999) 3533.
20) A. Suzuki, A. Endo and K. Tanaka: J. Phys. Soc. Jpn. **68** (1999) 3623.
21) A. L. Efros and B. I. Shklovskii: J. Phys. C **8** (1975) L49.
22) K. M. Abkemeier, C. J. Adkins, R. Asal and E. A. Davis: J. Phys.: Condens. Matt. **4** (1992) 9113.
23) B. L. Altshuler and A. G. Aronov: Solid State Commun. **30** (1979) 115.
24) R. Asal, S. H. Baker, S. J. Gurman, S. C. Bayliss and E. A. Davis: J. Phys.:Condens. Matt. **4** (1992) 7169.
25) J. F. Graczyk: Phys. Stat. Sol. A **55** (1979) 231.
26) D. A. Drabold and J. Dong: J. Non-Cryst. Solids **227–230** (1998) 153.
27) A. F. Ioffe and A. R. Regel: Prog. Semiconductors **4** (1960) 237.

Journal of the Physical Society of Japan
Vol. 69, No. 3, March, 2000, pp. 785-795

Magnetic Properties of the Hubbard Model on Three-Dimensional Lattices: Fluctuation-Exchange and Two-Particle Self-Consistent Studies

Ryotaro ARITA, Shigeki ONODA[1], Kazuhiko KUROKI and Hideo AOKI

Department of Physics, University of Tokyo, Hongo, Tokyo 113-0033
[1]*Institute for Solid State Physics, University of Tokyo, Roppoingi, Tokyo 106-8666*

(Received October 13, 1999)

The relation between three-dimensional lattice structure and magnetism in correlated electron systems is explored for face centered cubic (FCC), body centered cubic (BCC), and simple cubic (SC) lattices. In particular, we question which lattice structure has the strongest tendency toward the ferromagnetism or antiferromagnetism. We employ the Hubbard model to calculate the spin susceptibility and the single-particle spectrum with the fluctuation-exchange (FLEX) and the two-particle self-consistent (TPSC) approximations in the weak coupling regime. We have shown that (i) ferromagnetic spin fluctuations become dominant when the Fermi level lies around a sharp peak (divergence) in the density of states ($D(E)$) near the bottom of the band, which occurs for FCC with/without next nearest neighbor hoppings (t') or BCC with an appropriate value of t'. Among the cases studied, the ferromagnetic fluctuation is found to be the strongest for FCC with a finite t'. (ii) When the peak in $D(E)$ resides around the band center as in bipartite SC or BCC, antiferromagnetic fluctuations become dominant when the band is close to the half-filling, with the fluctuation being much stronger in BCC.

KEYWORDS: three-dimensional Hubbard model, ferromagnetism, antiferromagnetism, fluctuation exchange approximation, two-particle self-consistent approximation

§1. Introduction

The metallic ferromagnetism in repulsively interacting electron systems is among central problems in solid state physics, but is still some way from a complete understanding despite a long history of investigations. After the seminal papers by Kanamori,[1)] by Hubbard,[2)] and by Gutzwiller[3)] appeared back in the 1960's, the single-band Hubbard model has been studied intensively to understand metallic ferromagnetism. Although it is a simplest one conceivable, the model can still harbor insights into the fundamental mechanism for an itinerant ferromagnetism in correlated electron systems.

Historically, a guiding principle for realizing ferromagnetic states was provided by Stoner's mean field theory, which suggests that the ferromagnetic state should be favored for large enough interaction and/or density of states (DOS) at the Fermi level. Kanamori[1)] elaborated this argument with the T-matrix approximation to show that the ferromagnetic states are indeed favored when a peak in the DOS around the Fermi level is embedded around the bottom of the wide band. However, for general band filling, the extent to which the T-matrix approximation is valid is not clear.

As a different avenue along this line, rigorous results were recently obtained for ferromagnetism on specific lattices having flat bands. Lieb[4)] has shown that, when we have a bipartite lattice with different numbers of sublattice sites, the ground state at half filling should be ferrimagnetic for arbitrary magnitudes of the repulsion, U. Different numbers of sublattice sites imply that there is a flat band(s) in the one-electron band structure, or a delta-function density of states. Mielke and Tasaki[5)] then proved the existence of ferromagnetic ground states in systems with flat band for more general classes of lattices.

Going back to ordinary lattices, one can then look for divergences in the DOS to realize a ferromagnetic state in the Hubbard model. For three-dimensional lattices, the divergence occurs for the face centered cubic (FCC) lattice (where the DOS diverges at the band bottom, or above the bottom if we include next-nearest neighbor hopping, t') or for the body centered cubic (BCC) lattice (where the DOS diverges at the center due to the electron-hole symmetry, or away from the center if we include an appropriate value of t'). Our question here is 'among the lattice structures having sharply peaked (divergent) DOS's which one has the strongest tendency toward ferromagnetism?'. While the fully polarized ground state is expected to be favored when the DOS diverges near the bottom of the band, the tendency toward the ferromagnetic instabilities at finite temperatures is a non-trivial problem, because T_C of a system whose ground state is fully polarized is not necessarily higher than that of a system whose ground state is partially polarized.

As the background for the problem we can first recapitulate how the link between the lattice structure and the ferromagnetism has been understood in terms of the Hubbard model.[6)] The link may be tested accurately in one-dimensional (1D) systems, since the density matrix renormalization group (DMRG) method developed